Rapid Communications

# Nonlinear optical processes driven by superfluorescent fields and their controllability with external laser fields

Kenta Kitano,* Masataka Sato, Yuki Komasaka, and Haruka Maeda
*Department of Physics and Mathematics, Aoyama Gakuin University, Kanagawa 252-5258, Japan*

(Received 11 May 2020; accepted 25 August 2020; published 11 September 2020)

We investigated nonlinear optical processes driven by superfluorescent (SF) fields and their controllability with external laser fields. Cesium atoms were excited from the $6S$ ground state to the $8P$ state by a femtosecond laser pulse. The cascaded SF decay, $8P \rightarrow 8S \rightarrow 7P$, created coherence between the $7P$ and ground states, and led to the emission of a 455-nm pulse. A nanosecond laser pulse was applied to switch the $8S \rightarrow 7P$ transition to the $8S \rightarrow 6P$ one and newly generate an 852-nm pulse. At the same time, the nanosecond pulse suppressed the 852-nm emission through the inhibition of the development of the SF field between the $8P$ and $8S$ states, which led to the saturation of the 852-nm power with the increase of the nanosecond pulse power. The presented results offer an approach to investigate cooperative radiation processes in many-body systems and to develop an alternate light source.

DOI: 10.1103/PhysRevA.102.031101

An ensemble of two-level systems prepared in the excited state can evolve into the superradiant state in which dipoles of individual systems are coupled through spontaneous radiation and oscillate in phase with one another [1]. The superradiant state emits a coherent pulse called superfluorescence (SF), which has been observed in a variety of physical systems such as hot atoms and molecules [2–4], atoms embedded in planar cavities [5], electrons in semiconductor quantum wells [6], trapped ions [7], circuit QED [8], nitrogen-vacancy centers in diamond [9], and atoms in optical cavities [10]. Similar phenomena have also been demonstrated in a Bose-Einstein condensate, where a spontaneous Raman process produces macroscopic coherence of matter waves both with [11] and without cavities [12].

To generate SF, the preparation timescale should be sufficiently shorter than that of the SF dynamics [13]. Otherwise, spontaneous evolution into the superradiant state will be disturbed by the excitation process. Advances in ultrashort pulse technology in past decades have enabled us to produce and analyze ultrafast SF down to the picosecond timescale [3,14].

When SF occurs between two excited states in a multilevel system, which is often the case in gaseous medium, the SF initiates the next occurrence of SF in a cascading manner. Furthermore, when the SF dynamics occurs over a timescale of less than several nanoseconds, which is the typical Doppler dephasing time of electronic transitions in gaseous medium, the SF is accompanied by an additional emission originating from the coherence between the ground state and the excited state where the SF dynamics ended. Yoked SF (YSF) was the first demonstration of this phenomenon [14–17]. In YSF, three-level systems are initially prepared in superpositions of the ground and excited states. The SF from the transition between the excited and medium states is accompanied by coherent emission from the transition between the medium and ground states. More generally, YSF can be considered as one example of nonlinear optical processes driven by SF fields, which we refer to as "SF nonlinear optical processes."

Most research on SF or SF nonlinear optical processes has focused on how the coherence is spontaneously developed under field-free conditions. To give a detailed insight into these behaviors, it is important to investigate their controllability by external fields. Although this remains a challenging task, a few works have been reported. The phase [18] and intensity [19] of SF fields have been successfully controlled by applying a well-characterized seed pulse resonant with the SF fields. The transition from YSF to superradiance has been observed by applying a driving field to transfer population from the initial state of the YSF transition to another state [20]. In a theoretical study, the SF intensities in the V and $\Lambda$ configurations have been modulated by applying a resonant field that couples the initial or final states of the SF transition to another state [21]. It should be emphasized that different phenomena and their associated controllability will be found depending on how and on which states the external field acts.

A new scheme for SF nonlinear optical processes in which one-photon absorption was followed by cascaded SF and YSF to the ground state was reported [22]. Inspired by this, we applied a similar scheme but with an external field that acted on the second transition of the cascaded SF. We studied atomic cesium (Cs) vapor in a gas cell. As shown in Fig. 1(a), the atoms were excited from the $6S$ ground state to the $8P_{3/2}$ excited state via one-photon absorption by a femtosecond laser pulse, creating a superposition between the two states. The subsequent cascaded SF decay, $8P_{3/2} \rightarrow 8S \rightarrow 7P_{3/2}$, created coherence between the $7P_{3/2}$-$6S$ states, which induced a 455-nm emission, that is, YSF. We applied a nanosecond laser pulse as a control pulse with a frequency resonant to the $8S$-$6P_{3/2}$ transition frequency. Through applying this field, an 852-nm emission appeared as a consequence of the SF nonlinear optical process. We refer to this as "forced SF (FSF)" in this Rapid Communication. We investigate how the YSF

*kkitano@phys.aoyama.ac.jp

 

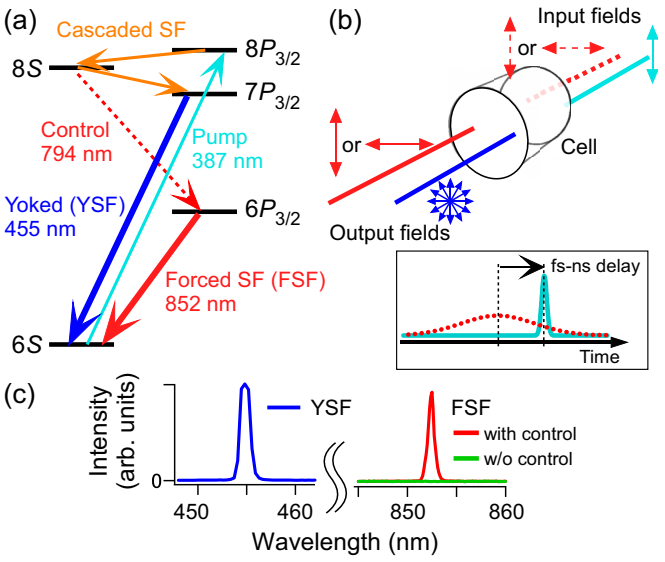


FIG. 1. (a) Energy diagram of Cs atoms and related transitions. (b) The experimental scheme to control the SF nonlinear process. (c) YSF and FSF spectra.

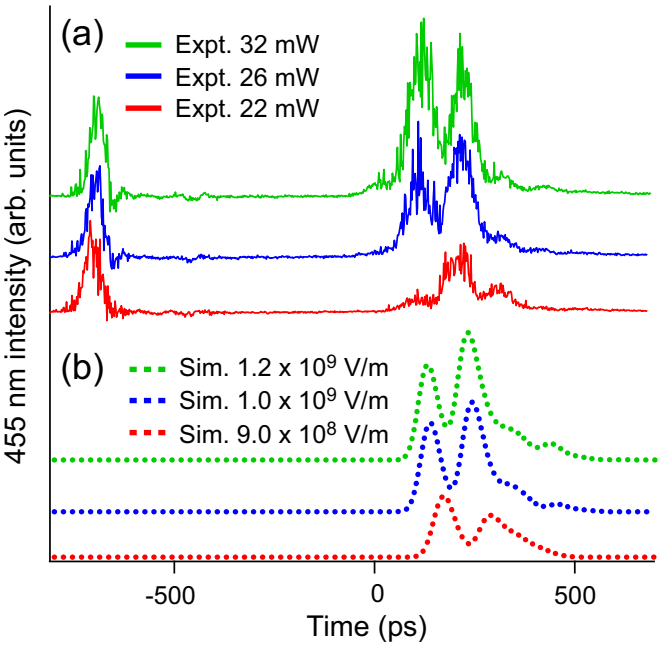


FIG. 2. (a) Experimental results for the temporal profiles of the 455-nm emission at different pump pulse powers. (b) Simulated results at different pump pulse intensities, which reproduce the experimental results.

(the 455-nm emission) and FSF (the 852-nm emission) coexist or dominate over the other under different conditions of the control pulse. Moreover, we clarify the two opposing effects that the control pulse has. At low field intensities, the control pulse induces the $8S$-$6P_{3/2}$ transition and enhances the FSF. However, at high field intensities, it inhibits the development of the SF field between the $8P_{3/2}$-$8S$ states and suppresses the FSF. The power of the FSF therefore saturates with the increase of control pulse power. This is demonstrated in both the experimental and simulation results.

A schematic of the experimental setup is depicted in Fig. 1(b). We employed the second harmonic of a 100-fs Ti:sapphire laser pulse as the pump pulse with a central wavelength of 387 nm, a repetition rate of 1 kHz, and a maximum pulse energy of 40 $\mu$J. For the control pulse, we employed a Nd:YAG pumped dye laser with a pulse width of 5 ns, a central wavelength of 794 nm, a repetition rate of 20 Hz, and a maximum pulse energy of 350 $\mu$J. The pump pulse was vertically polarized. The polarization of the control pulse was set parallel or perpendicular to that of the pump pulse. The relative delay between the pump and control pulses was electronically controlled. Both the beams were collimated, and collinearly fed into a 60-mm-long Pyrex glass cell containing Cs vapor. The FWHM of the pump beam was 0.58 mm, while that of the control beam was slightly larger. The cell temperature was monitored through its window and maintained at 115 °C. Various types of optical filters were used to block the pump and control beams while allowing the transmission of the YSF and FSF.

We first recorded the 455-nm emission without the control pulse. The spectrum and beam profile at 250 mm away from the end face of the cell are shown in Figs. 1(c) and 4(a), respectively. The beam divergence was measured to be 2.4 mrad. We approximated the wave-vector mismatch $\Delta k$ in the four-wave mixing (FWM) process by $2\pi(1-\cos\theta)/\lambda$, where $\lambda$ and $\theta$ are the wavelength of the YSF or FSF and the angle of each wave-vector direction from the propagation axis of the pump beam, respectively. The beam divergence of the 455-nm emission is then expected to be 3.1 mrad, which agrees with the experimental result. The polarization of the 455-nm emission was, on the average, random, which can be explained as follows: The polarization of the SF from the $8S$-$7P_{3/2}$ transition should be arbitrary because the $8S$ electronic state is spherically symmetrical [23]. Furthermore, as the SF from the $8S$-$7P_{3/2}$ transition and the 455-nm emission are correlated with each other, the polarization of the former might be imprinted on the latter, which we will prove in future experiments. It should be noted that the polarization of the control pulse is actually imprinted on that of the FSF, which is shown later in this Rapid Communication. Figure 2(a) shows the temporal profiles of the 455-nm emission recorded by a sampling oscilloscope at different pump pulse powers. In addition to the 455-nm emission, the reference pulse was always monitored, which is seen at around $-700$ ps in the figure. To analyze these results, we simulated the time evolution of the atomic density operator $\rho$ and the Rabi frequency $\Omega_{\alpha\beta} = \mu_{\alpha\beta}\varepsilon/\hbar$, where $\mu_{\alpha\beta}$ and $\varepsilon$ are, respectively, the transition dipole moment between the two states labeled as $\alpha$ and $\beta$, and the electric field envelope. We applied semiclassical theory and numerically solved the coupled Maxwell-Bloch equations for the $6S$, $6P_{3/2}$, $6P_{1/2}$, $7P_{3/2}$, $7P_{1/2}$, $8S$, $8P_{3/2}$, and $8P_{1/2}$ states [14,17]. The initial state of $\rho$ was assumed to be the coherent superposition created after irradiation by the pump pulse. For the boundary condition, we introduced the constant electric field envelope for each Rabi frequency estimated from the spontaneous emission rate into the solid angle of the YSF. The equation is given by

$$\varepsilon_{\mathrm{const}} = \sqrt{\frac{N\hbar\omega\Omega_{\mathrm{so}}L}{T_{\mathrm{sp}}c\varepsilon_0}}, \tag{1}$$

where $\omega$, $\Omega_{so}$, $L$, $T_{sp}$, $N$, $c$, and $\epsilon_0$ are the angular frequency, the solid angle of the YSF, the sample length, the lifetime of an isolated atom, the atomic number density, the speed of light, and the vacuum permittivity, respectively. All the Rabi frequencies were uniformly reduced by a factor of 5 to match the experimental results. The simulated results are indicated in Fig. 2(b) by dashed lines and reproduce the characteristic double peaks in the experimental results. These double peaks are not directly related to the coherent ringing that often appears in SF pulses. Coherent ringing accompanies synchronized Rabi oscillations as well as phase inversion of polarization between two related states [13]. In the simulation results shown in Fig. 2(b), the population of the ground state is almost unchanged during the 455-nm emission, and the phase of the 455-nm emission is constant. Furthermore, we confirmed with another simulation that the double peaks appear when the temporal profile of the SF field between the $8S$-$7P_{3/2}$ transition is distorted during propagation [24]. These results indicate that the double peaks in Fig. 2(b) originate in the propagation effect in multilevel systems. The electric field envelopes used in the simulation were 1.5 times larger than that estimated from the experimental parameters.

Next, we set the pump pulse power to 26 mW and irradiated the atoms with the control pulse. We newly observed an 852-nm emission. These spectra are shown in Fig. 1(c). The 852-nm beam divergence was measured to be 3.7 mrad, which is within the calculated value of 4.3 mrad for the FWM process. We measured the 852-nm polarization using a Glan-Thompson polarizer. Figure 3(a) shows the transmitted powers of the 852-nm emission and the control pulse as functions of the polarizer angle. As expected, the polarization of the 852-nm emission was identical to that of the control pulse regardless of whether the control pulse was horizontally or vertically polarized. For the remainder of this Rapid Communication, the polarization of the control pulse was set parallel to that of the pump pulse. Figure 3(b) shows the measured 852-nm power as a function of the control pulse power and the relative delay of the pump pulse with respect to the control pulse [see Fig. 1(b)]. The 852-nm emission appeared within a range of 10 ns of the femtosecond-nanosecond delay. This is reasonable considering the 5-ns pulse width of the control pulse. At any given value of the femtosecond-nanosecond delay, the 852-nm power first increased with the control pulse power. However, the slope depends on the femtosecond-nanosecond delay and is steepest at around −3 ns, suggesting that the control pulse acted on the cascaded SF process most effectively when the pump pulse slightly preceded the control pulse. This can be explained by considering the development of the SF field during the time delay after the excitation by the pump pulse. Figure 3(c) shows the variation of the 852-nm power with the control pulse power at −2.5 ns of the femtosecond-nanosecond delay in Fig. 3(b). Clearly, the 852-nm power saturated at around 2 mW of the control pulse power, and started to decrease from there. This behavior is discussed in detail in the final part of this Rapid Communication.

We conducted another set of experiments in which the 455- and the 852-nm temporal profiles and their images were recorded at different control pulse powers indicated in Fig. 3(c). The results of the 455- and 852-nm emissions are summarized in Figs. 4(a)–4(c) and 4(d)–4(f), respectively.

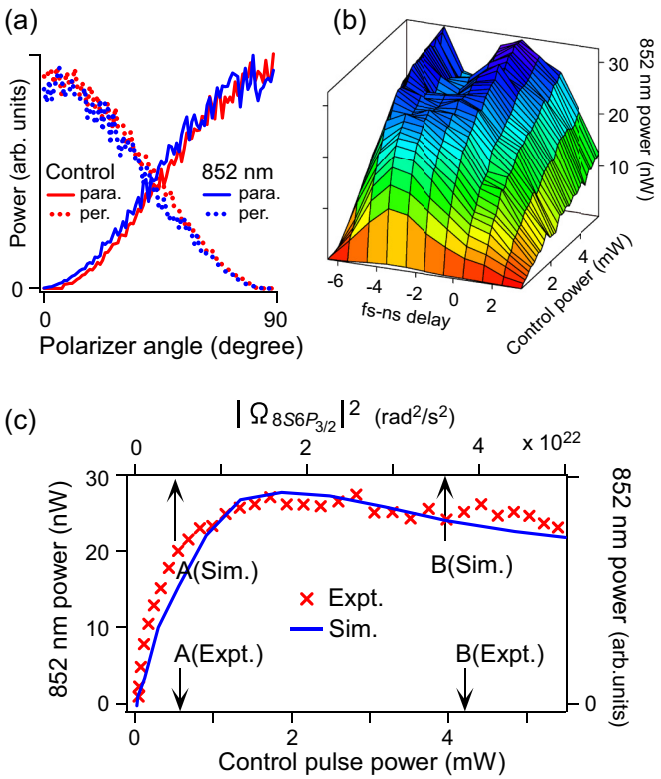


FIG. 3. (a) Transmitted powers of the 852-nm emission and control pulse with respect to the polarizer angle. (b) The measured power of the 852-nm emission plotted as a function of the femtosecond-nanosecond delay and the control pulse power. (c) Experimental (simulated) results of the 852-nm power plotted on the left (right) axis as a function of the control pulse power (intensity) on the bottom (top) axis. The femtosecond-nanosecond delay is fixed at −2.5 ns in the experimental result.

Figures 4(a) and 4(d) show the results without the control pulse. Figures 4(b) and 4(e) correspond to the results recorded at the control pulse power indicated by A(Expt.) in Fig. 3(c), while Figs. 4(c) and 4(f) correspond to the results indicated by B(Expt.) there. For the 455-nm emission, the double peak in Fig. 4(a) disappears in Fig. 4(b), and the signal there lasts almost 1 ns. Further increasing the control pulse power [Fig. 4(c)] substantially suppressed the signal intensity. For the 852-nm emission, we observed no signal without the control pulse [Fig. 4(d)]. After adding the control pulse, the signal appeared in Fig. 4(e) and its intensity increased in Fig. 4(f). The pulse widths are estimated to be several hundreds of picoseconds, which is considerably shorter than the control pulse width of 5 ns. This clearly demonstrates that the 852-nm emission originated from the SF nonlinear optical process.

To analyze these results, we performed simulations by replacing the electric field envelope in Eq. (1) with that of the control pulse. The results for the 455- and the 852-nm emissions are shown in Figs. 4(g)–4(i) and Figs. 4(j)–4(l), respectively. In order to show the detailed temporal structure, we did not convolute the simulated results. For the 455-nm emission, the signal in Fig. 4(h) is delayed and its pulse width is elongated when compared to the signal in Fig. 4(g). This

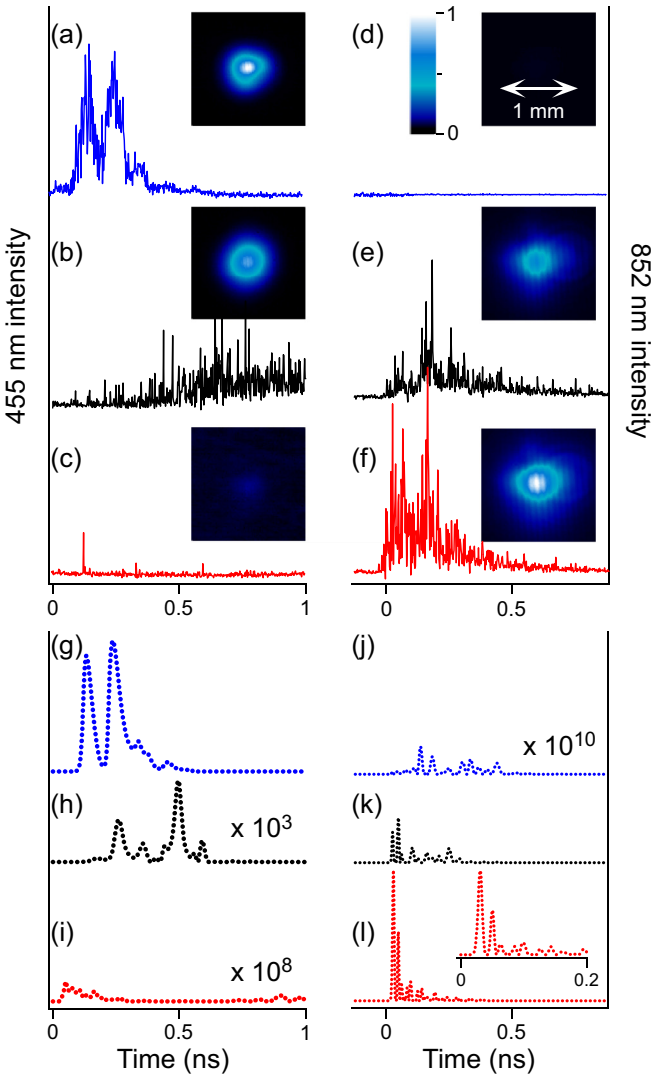


FIG. 4. (a)–(f) Experimental results for the 455-nm emission (a)–(c) and the 852-nm emission (d)–(f). (a) and (d) were recorded without the control pulse. (b) and (e), and (c) and (f) were recorded with the control pulse, of which the powers are indicated by A(Expt.) and B(Expt.) in Fig. 3(c), respectively. (g)–(l) Simulated results of the 455-nm emission (g)–(i) and the 852-nm emission (j)-(l). (g) and (j) were recorded without the control pulse. (h) and (k), and (i) and (l) were recorded with the control pulse, of which the intensities are indicated by A(Sim.) and B(Sim.) in Fig. 3(c), respectively. (h) and (i) are vertically magnified by factors of $10^3$ and $10^8$, respectively, with respect to (g), and (j) is vertically magnified by a factor of $10^{10}$ with respect to (k) and (l).

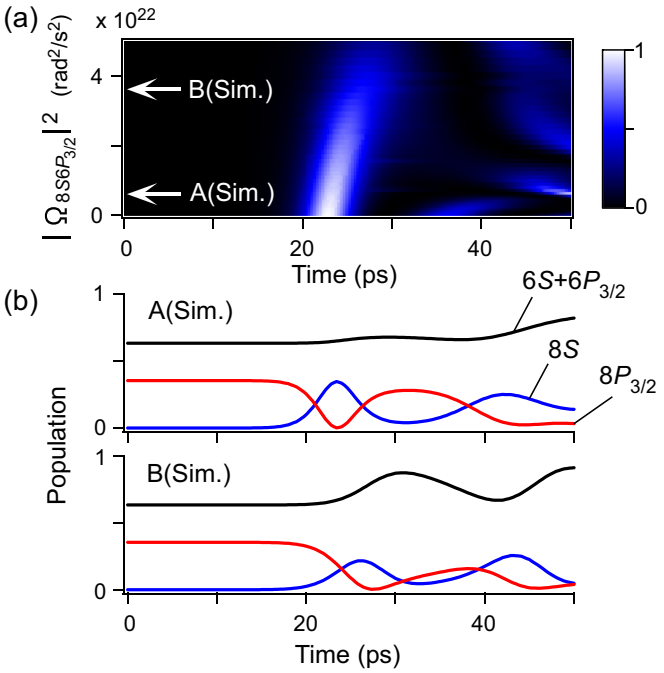


FIG. 5. (a) The simulated result of the SF intensity from the $8P_{3/2}$-$8S$ transition, $|\Omega_{8P_{3/2}8S}|^2$, plotted as a function of the time and the control pulse intensity, $|\Omega_{8S6P_{3/2}}|^2$. (b) The populations of the $8P_{3/2}$ state, the $8S$ state, and the sum of the $6S$ and $6P_{3/2}$ states plotted as a function of time at the control pulse intensities indicated by the white arrows in (a) and the black arrows in Fig. 3(c).

qualitatively reproduces the observed results in Figs. 4(a) and 4(b). However, the signal intensity in Fig. 4(h) is reduced by a factor of $10^3$ with respect to that in Fig. 4(g), which differs from the experimental results. This disagreement might be due to incoherent amplification processes such as amplified spontaneous emission, which were not included in the simulation. For the 852-nm emission, the signal intensity is significantly weaker without the control pulse [Fig. 4(j)]. Adding the control pulse, the 852-nm emission appears in Fig. 4(k), and its intensity increases along with the control pulse power in Fig. 4(l), which agrees with the experimental results. On the other hand, the pulse width in Fig. 4(l) is smaller than that in Fig. 4(f). This discrepancy might be due to the intensity fluctuation of the control pulse. As shown in the inset of Fig. 4(l), the 852-nm emission consists of several peaks. We confirmed that these structures vary sensitively with the control pulse intensity. Therefore, the pulse width could be elongated during the averaging procedure in the experiment. The electric field envelope used in the simulation was 0.6 times smaller than that estimated from the experimental parameters.

Finally, we discuss the saturation behavior of the 852-nm emission in Fig. 3(c). For this purpose, the simulated results exemplified in Figs. 4(j)–4(l) were integrated in the time domain and plotted in Fig. 3(c) as a function of the squared Rabi frequency of the control pulse. The simulated results successfully reproduced the observed results. The saturation behavior in the simulation can be understood by considering the two opposing effects of the control pulse. One effect of the control pulse is to induce the $8S$-$6P_{3/2}$ transition and generate the 852-nm emission. The 852-nm intensity increases along with the control pulse intensity, which gives the steep slope for control pulse intensity $<1.5\times10^{22}$ (rad$^2$/s$^2$) in Fig. 3(c). The other effect of the control pulse is to inhibit the development of the $8P_{3/2}$-$8S$ SF field by transferring the population from the $8S$ to the $6P_{3/2}$ state. We will explain this in more detail. Figure 5(a) shows the simulated intensity of the $8P_{3/2}$-$8S$ SF field as a function of the time and the control pulse intensity. By increasing the control pulse intensity, the first peak at around 23 ps is delayed and its intensity decreases. As expected, the intensity of this peak is almost unchanged at the control pulse intensity of A(Sim.) in the figure which is

located on the positive slope in Fig. 3(c), while it is severely weakened at the intensity of B(Sim.) in the figure which is located on the negative slope in Fig. 3(c). In Fig. 5(b), the populations of the $8P_{3/2}$ state, the $8S$ state, and sum of the $6S$ and $6P_{3/2}$ states are plotted as a function of time at the control pulse intensities of A(Sim.) and B(Sim.). As expected, a larger fraction of the population is dumped to the lower states (the $6S$ and $6P_{3/2}$ states) for the case of B(Sim.) than for the case of A(Sim.). This inhibition resembles the one discussed in the YSF [15], but appears in a different manner. Moreover, the inhibition might be explained from the perspective of odd-photon destructive interference [25]. It should be stressed that the SF fields develop along with the propagation whereas the control pulse field is almost unchanged. Therefore, the saturation behavior depends on the sample length [24].

In conclusion, we investigated the SF nonlinear optical process in cesium, where one-photon absorption was followed by cascaded SF and YSF. The SF nonlinear optical process was controlled by the external laser field, generating the FSF. The timescale of the FSF was sufficiently shorter than the control pulse width, indicating that ultrafast SF dynamics could be controlled even with intense continuous laser fields. The observed power saturation of the FSF is explained by considering the two opposing effects of the control pulse, namely, the enhancement of the FSF field through the population transfer and its suppression through the inhibition of SF field development. These results show how to control and utilize the interplay between spontaneously developed and externally imparted coherence, and pave the way to the development of various types of SF nonlinear optical processes.

This work was financially supported by JSPS KAKENHI Grant No. 18K04984 and JKA and its promotion funds from KEIRIN RACE.

[1] R. H. Dicke, Phys. Rev. **93**, 99 (1954).
[2] N. Skribanowitz, I. P. Herman, J. C. MacGillivray, and M. S. Feld, Phys. Rev. Lett. **30**, 309 (1973); H. M. Gibbs, Q. H. F. Vrehen, and H. M. J. Hikspoors, *ibid.* **39**, 547 (1977).
[3] M. Nagasono, J. R. Harries, H. Iwayama, T. Togashi, K. Tono, M. Yabashi, Y. Senba, H. Ohashi, T. Ishikawa, and E. Shigemasa, Phys. Rev. Lett. **107**, 193603 (2011).
[4] Y. Liu, P. Ding, G. Lambert, A. Houard, V. Tikhonchuk, and A. Mysyrowicz, Phys. Rev. Lett. **115**, 133203 (2015); A. Zhang, Q. Liang, M. Lei, L. Yuan, Y. Liu, Z. Fan, X. Zhan, S. Zhuang, C. Wu, Q. Gong, and H. Jiang, Opt. Express **27**, 12638 (2019).
[5] R. Röhlsberger, K. Schlage, B. Sahoo, S. Couet, and R. Rüffer, Science **328**, 1248 (2010).
[6] Q. Zhang, T. Arikawa, E. Kato, J. L. Reno, W. Pan, J. D. Watson, M. J. Manfra, M. A. Zudov, M. Tokman, M. Erukhimova, A. Belyanin, and J. Kono, Phys. Rev. Lett. **113**, 047601 (2014).
[7] J. Eschner, Ch. Raab, F. Schumidt-Kaler, and R. Blatt, Nature (London) **413**, 495 (2001); R. G. DeVoe and R. G. Brewer, Phys. Rev. Lett. **76**, 2049 (1996).
[8] J. A. Mlynek, A. A. Abdumalikov, C. Eichler, and A. Wallraff, Nat. Commun. **5**, 5186 (2014).
[9] A. Angerer, K. Streltsov, T. Astner, S. Putz, H. Sumiya, S. Onoda, J. Isoya, W. J. Munro, K. Nemoto, J. Schmiedmayer, and J. Majer, Nat. Phys. **14**, 1168 (2018); C. Bradac, M. Johnsson, M. van Breugel, B. Baragiola, R. Martin, M. L. Juan, G. Brennen, and T. Volz, Nat. Commun. **8**, 1205 (2017).
[10] J. Kim, D. Yang, S. Oh, and K. An, Science **359**, 662 (2018); J. G. Bohnet, Z. Chen, J. M. Weiner, D. Meiser, M. J. Holland, and J. K. Thompson, Nature (London) **484**, 78 (2012).
[11] S. Bux, C. Gnahm, R. A. W. Maier, C. Zimmermann, and P. W. Courteille, Phys. Rev. Lett. **106**, 203601 (2011).
[12] S. Inouye, A. P. Chikkatur, D. M. Stamper-Kurn, J. Stenger, D. E. Pritchard, and W. Ketterle, Science **285**, 571 (1999).
[13] M. S. Feld and J. C. MacGillivray, *Coherent Nonlinear Optics, Superradiance* (Springer-Verlag, Berlin, 1980).
[14] L. Yuan, B. H. Hokr, A. J. Traverso, D. V. Voronine, Y. Rostovtsev, A. V. Sokolov, and M. O. Scully, Phys. Rev. A **87**, 023826 (2013); G. O. Ariunbold, M. M. Kash, V. A. Sautenkov, H. Li, Y. V. Rostovtsev, G. R. Welch, and M. O. Scully, *ibid.* **82**, 043421 (2010).
[15] J. H. Brownell, X. Lu, and S. R. Hartmann, Phys. Rev. Lett. **75**, 3265 (1995).
[16] K. Kitano and H. Maeda, Opt. Express **25**, 23826 (2017); G. O. Ariunbold, V. A. Sautenkov, and M. O. Scully, Opt. Lett. **37**, 2400 (2012); G. O. Ariunbold, M. M. Kash, V. A. Sautenkov, H. Li, Y. V. Rostovtsev, G. R. Welch, and M. O. Scully, J. Opt. Soc. Am. B **28**, 515 (2011); D. Felinto, L. H. Acioli, and S. S. Vianna, Opt. Lett. **25**, 917 (2000); A. I. Lvovsky, S. R. Hartmann, and F. Moshary, Phys. Rev. Lett. **82**, 4420 (1999); A. I. Lvovsky, Ph.D. thesis, Columbia University, 1998.
[17] K. Kitano and H. Maeda, Phys. Rev. A **100**, 041803(R) (2019); **97**, 063418 (2018).
[18] G. A. Mesyats, N. S. Ginzburg, A. A. Golovanov, G. G. Denisov, I. V. Romanchenko, V. V. Rostov, K. A. Sharypov, V. G. Shpak, S. A. Shunailov, M. R. Ulmaskulov, M. I. Yalandin, and I. V. Zotova, Phys. Rev. Lett. **118**, 264801 (2017).
[19] Z. Wang, H. Li, W. Feng, X. Song, C. Song, W. Liu, Q. Guo, X. Zhang, H. Dong, D. Zheng, H. Wang, and D. W. Wang, Phys. Rev. Lett. **124**, 013601 (2020).
[20] Z. Yi, P. K. Jha, L. Yuan, D. V. Voronine, G. O. Ariunbold, A. M. Sinyukov, Z. Di, V. A. Sautenkov, Y. V. Rostovtsev, and A. V. Sokolov, Opt. Commun. **351**, 45 (2015).
[21] M. Macovei, J. Evers, and C. H. Keitel, Phys. Rev. Lett. **91**, 233601 (2003).
[22] J. R. Harries, H. Iwayama, S. Kuma, M. Iizawa, N. Suzuki, Y. Azuma, I. Inoue, S. Owada, T. Togashi, K. Tono, M. Yabashi, and E. Shigemasa, Phys. Rev. Lett. **121**, 263201 (2018).
[23] A. Crubellier, S. Liberman, and P. Pillet, Phys. Rev. Lett. **41**, 1237 (1978).
[24] See Supplemental Material at http://link.aps.org/supplemental/10.1103/PhysRevA.102.031101 for additional simulation results.
[25] M. G. Payne, L. Deng, and W. R. Garrett, Phys. Rev. A **58**, 1361 (1998); L. Deng, W. R. Garrett, M. G. Payne, and D. Z. Lee, *ibid.* **54**, 4218 (1996); W. R. Garrett, Phys. Rev. Lett. **70**, 4059 (1993).